

Optimising quantum tomography via shadow inversion

Andrea Caprotti^{✉*} and Joshua Morris^{✉†}

University of Vienna, Faculty of Physics, Vienna Center for Quantum Science and Technology (VCQ), Boltzmanngasse 5, 1090 Vienna, Austria and

University of Vienna, Vienna Doctoral School in Physics, Boltzmanngasse 5, 1090 Vienna, Austria

Borivoje Dakić^{✉‡}

University of Vienna, Faculty of Physics, Vienna Center for Quantum Science and Technology (VCQ), Boltzmanngasse 5, 1090 Vienna, Austria and

Institute for Quantum Optics and Quantum Information (IQOQI), Austrian Academy of Sciences, Boltzmanngasse 3, 1090 Vienna, Austria.

In quantum information theory, the accurate estimation of observables is pivotal for quantum information processing, playing a crucial role in compute and communication protocols. This work introduces a novel technique for estimating such objects, leveraging an underutilised resource in the inversion map of classical shadows that greatly refines the estimation cost of target observables without incurring any additional overhead. A generalised framework for computing and optimising additional degrees of freedom in the homogeneous space of the shadow inversion is given that may be adapted to a variety of near-term problems. In the special case of local measurement strategies we show feasible optimisation leading to an exponential separation in sample complexity versus the standard approach and in an exceptional case we give non-trivial examples of optimised post-processing for local measurements, achieving the same efficiency as the global Cliffords shadows.

INTRODUCTION

Quantum state tomography with classical shadows [1], initially motivated by the seminal work of Aaronson [2], represents a significant advancement in the realm of quantum information processing, particularly in the efficient characterisation of quantum systems. This technique, developed as a solution to the prohibitive resource requirements of full quantum state tomography has since seen a plethora of modifications [3–23], which all seek to provide a viable alternative for obtaining meaningful information about quantum states with substantially reduced computational and experimental overhead [24–35]. Naturally, the main focus has been the ‘quantum’ element of the procedure as this is where most practical efforts are stymied, either in gate or sample complexity. Other than machine learning [26, 36] and adaptive techniques [33, 37], little thought has been put towards explicit optimisation of the classical postprocessing with it often being treated as a mostly fixed step.

At the core of shadow tomography lies the concept of constructing these aforementioned shadows; efficiently representable compressed classical descriptions of quantum states. These shadows are generated through a process involving random measurements on copies of a state, followed by classical processing to reconstruct a succinct representation of the state, the ‘shadow’. These classical shadows, though not providing a complete description of the quantum state, contain enough information to estimate a wide range of properties with high accuracy when an appropriate POVM is used. An archetypal example is the set of measurements performed by random perturbations sampled from the Clifford group [38, 39] followed by a computational basis measurement

$$\mathcal{C}_N = \{T \in SU(2^N) \mid T P_N T^\dagger \in \mathcal{P}_N\} / U(1), \quad (1)$$

for all P_N , the set of Pauli operators on N qubits. Critically for shadow tomography, we have that the Clifford group constitutes a 2, 3-design [38] i.e., it can reproduce the statistical properties of the full set of unitaries up to the second and third moment. It is this that forms the basis upon which shadow tomography derives its impressive performance, implementing a map whose consequent inverse lies at the core of efficient estimation with classical shadows. If U_k are elements of the N qubit Clifford group and Π_ℓ are computational measurement projectors all acting on an input N qubit quantum state then

$$\mathcal{M}[\rho] = \frac{1}{|\mathcal{C}_N|} \sum_{k=1}^{|\mathcal{C}_N|} \sum_{\ell=1}^{2^N} T_{k\ell} \rho T_{k\ell}^\dagger = \lambda \rho + (1-\lambda) \text{tr}(\rho) \frac{\mathbb{1}}{2^N}, \quad (2)$$

for $T_{k\ell} = U_k^\dagger \Pi_\ell U_k$. The inverse operation \mathcal{M}^{-1} may be easily computed to recover the input state ρ from the output \mathcal{M}^{-1} . Classical shadows’ great insight was to show that this inversion procedure remains effective even when only a tiny fraction of Clifford measurements are used in the above sum. This rapid convergence to a known configuration means the linear map of Eq. (2) may be readily inverted to recover the original state ρ . As shown in [1], the inverse map of Eq. (2) for global Clifford measurements on N qubits seems to easily appear as the inverse depolarising channel: $\mathcal{M}_N^{-1}(X) = (2^N + 1)X - \text{Tr}[X] \mathbb{1}_{2^N}$; in the case of tensor products of random single-qubit Pauli measurements, the corresponding inverted quantum channel reduces to $\mathcal{M}_{\mathcal{P}}^{-1} = \bigotimes_{i=1}^N \mathcal{M}_1^{-1}$.

In these cases, the inversion map takes a particularly simple form, and the estimation of consumed resources (sampling complexity) critically depends on it. Nevertheless, what is often neglected in studies is the fact that such a map is not unique, i.e., as long as the POVM used is overcomplete (in the operator, Hilbert-Schmidt space), an additional set of free parameters appear in the inversion process which may be op-

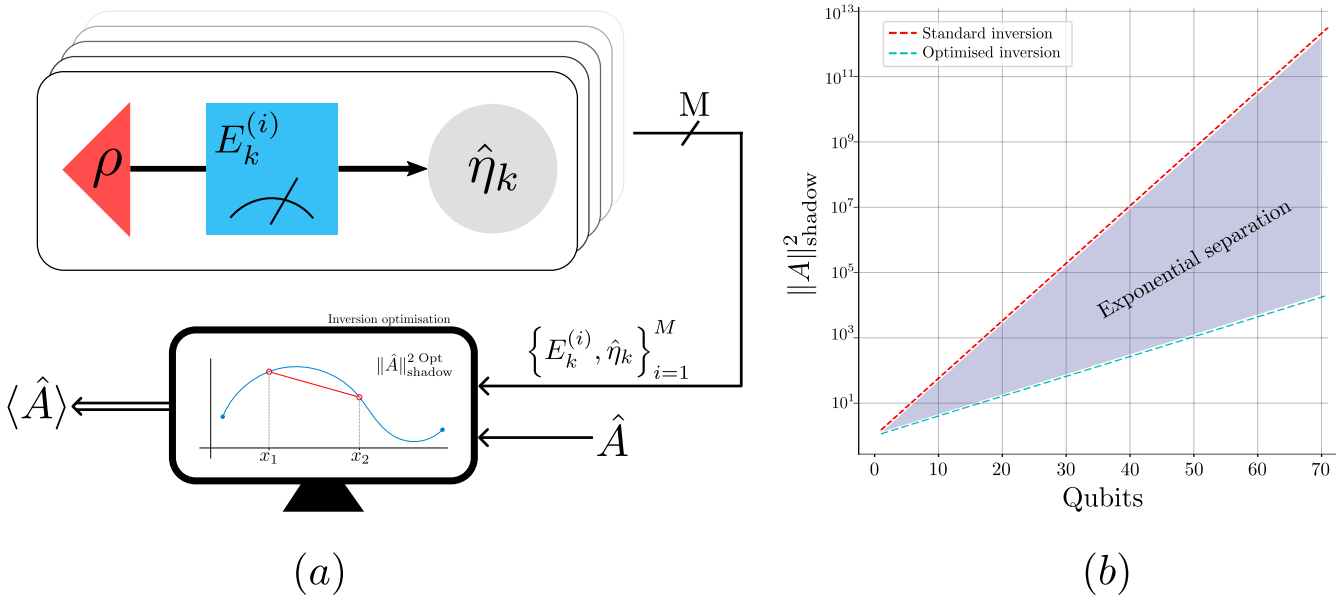


FIG. 1. (a) **Classical shadow tomography with optimised shadow inversion.** After a collection of M POVM outcomes have been acquired from a fixed quantum state, any estimation can be improved for a dynamic choice of target observable A by computing an optimal ‘inverse’ operation for that observable and POVM. (b) **Shadow norm for different strategies.** The shadow norm cofactor when optimised for certain target projectors, using local Pauli measurements on single qubits. The shadow norm for such an observable on N qubits is normally $(3/2)^N$ but when optimised over additional degrees of freedom can be shrunk to $(1.15)^N$. Though still exponential in the number of qubits, the optimised strategy is exponentially cheaper than standard classical shadow tomography with local measurements.

timised to improve the post-processing performance of the estimation procedure. Surprisingly, this has been only recently recognised in the literature [40] by employing the techniques of measurement dual frames. In this work, we demonstrate that such additional degrees of freedom reside in the homogeneous space, i.e. the general inverse map contains a free homogeneous component $\mathcal{M}^{-1} = \mathcal{M}_p^{-1} + \mathcal{M}_h^{-1}$ which can be further optimized. Our goal is to pursue such an optimisation by considering a hereto before missed resource in the tomography procedure that appears most vividly in classical shadows and the post-processing thereof. Though the natural choice of the inverse map (such as the one given above) is the inverse of the forward channel being applied, there is nothing that says it must be so. It is this inversion process, normally treated as a fixed mathematical procedure, that we aim to modify and improve upon. As long as the set of performed measurements is tomographically over-complete, the additional degrees of freedom may be exploited to reduce case-specific variance for a given observable. In doing so, we will show that an exponential improvement in estimations is possible compared to the standard choice of inverse map presented in the literature. With this novel approach to processing acquired quantum data, we open a new route to exploit areas where advantages may be gained without incurring an unacceptable resource cost.

SHADOW MAP INVERSION

We begin by describing a generalised procedure [27, 41], depicted in Figure 1(a) fulfilling the random measurement scheme with a fixed POVM $\{E_k\}_{k=1}^n$ on a d -dimensional system. The POVM elements sample randomly an unknown state ρ with probability $p_k = \text{Tr}[\rho E_k]$. These POVM elements span a subspace $\mathcal{V}_D = \text{Span}\{E_k\}_{k=1}^n$ in the Hilbert-Schmidt space (HS) of the dimension $|\mathcal{V}_D| = D$. Typically, $D = d^2$ (the entire HS space), but for the sake of generality, we shall keep $D \leq d^2$. Furthermore, we assume $D < n$, thus E_k forms an over-complete basis in \mathcal{V}_D . The estimation task aims to approximate the mean values of an observable $A \in \mathcal{V}_D$, i.e., $\langle A \rangle = \text{Tr}[A\rho]$. Note that $\langle A \rangle = \text{Tr}[A\bar{\rho}]$, with $\bar{\rho}$ being the projection of a quantum state ρ onto \mathcal{V}_D which follows directly from $A \in \mathcal{V}_D$. For the case of the entire HS space, we have $\bar{\rho} = \rho$. Similarly, the measured probabilities trivially satisfy $p_k = \text{Tr}[E_k\rho] = \text{Tr}[E_k\bar{\rho}]$. The post-processing task assigns a (matrix) estimator $\hat{\eta} \in \{\dots, \hat{\eta}_k, \dots\}$, i.e. each outcome E_k the corresponding matrix $\hat{\eta}_k$, which represents a single-shot approximation of $\bar{\rho}$. They can be calculated via an inversion map $\hat{\eta}_k = \mathcal{M}^{-1}(E_k)$ [1, 27] which we will show is not unique, i.e. $\mathcal{M}^{-1} = \mathcal{M}_p^{-1} + \mathcal{M}_h^{-1}$ with the latter (homogeneous) component containing auxiliary parameters that may be used as a free resource in post-processing.

The overall classical shadow itself is obtained by averaging over the estimators obtained from M random measurements: $M^{-1} \sum_s^M \hat{\eta}^{(s)}$. Assuming that all samples are i.i.d., the aver-

age value $\langle \hat{\eta} \rangle$ is immediately

$$\langle \hat{\eta} \rangle = \sum_{k=1}^n p_k \hat{\eta}_k = \sum_{k=1}^n \text{Tr}[\bar{\rho} E_k] \hat{\eta}_k = \bar{\rho}, \quad \forall \bar{\rho} \in \mathcal{V}_D. \quad (3)$$

This is the requirement on the estimator $\hat{\eta}$ such that the statistics of the shadow mimics, in expectation, that of the actual unknown state. With Eq. (3), the task of finding an inversion map can be made equivalent to identifying a dual frame to the POVM in space of operators [40]. Since the POVM forms an over-complete basis in \mathcal{V}_D , the solution to Eq. (3) is not unique. This multiplicity results in a set of free parameters, which becomes an extra resource that may be used in the post-processing component of an estimation to reduce the variance.

To achieve this, we now show a constructive method to recover families of equivalent classical shadows in terms of the POVM elements and their free parameters. We rely on an equivalent problem to Eq. (3), that is, to impose the equivalence between the expectation value of an observable A and the corresponding classical estimator $a = \text{Tr}[A \hat{\eta}]$:

$$\langle a \rangle = \text{Tr}[A \langle \hat{\eta} \rangle] = \sum_{k=1}^n p_k \text{Tr}[A \hat{\eta}_k] = \text{Tr}[\bar{\rho} A]. \quad (4)$$

It is instructive to express the operators as vectors in \mathcal{V}_D , i.e., for an operator $X \in \mathcal{V}_D$, we shall use the ket notation $|X\rangle\rangle$. We also identify an orthonormal basis $\beta_D = \{|B_j\rangle\rangle\}_{j=1}^D$ in \mathcal{V}_D .

The expectation value from Eq. (4) can be expressed as

$$\langle a \rangle = \sum_{k=1}^n \langle\langle A^\dagger | \eta_k \rangle\rangle \langle\langle E_k^\dagger | \rho \rangle\rangle = \langle\langle A^\dagger | \bar{\rho} \rangle\rangle \quad (5)$$

where $\langle\langle X | Y \rangle\rangle = \text{Tr}[X^\dagger Y]$ is the inner product in \mathcal{V}_D .

To guarantee the estimators are unbiased, the requirement reduces to a resolution of the identity in the subspace \mathcal{V}_D

$$\sum_{k=1}^n |\eta_k\rangle\rangle \langle\langle E_k^\dagger| = \sum_{k=1}^n |\eta_k\rangle\rangle \langle\langle E_k| \equiv \mathbb{1}_D, \quad (6)$$

which can be solved for $|\eta_k\rangle\rangle$ using $E_k^\dagger = E_k$. The last equation expressed in the basis β_D reads

$$\sum_{k=1}^n \langle\langle B_s | \hat{\eta}_k \rangle\rangle \langle\langle E_k | B_t \rangle\rangle = \sum_{k=1}^n L_{sk} R_{tk}^* = \delta_{st}, \quad (7)$$

with $L_{sk} = \langle\langle B_s | \hat{\eta}_k \rangle\rangle$ and $R_{tk} = \langle\langle B_t | E_k \rangle\rangle$. This implies the matrix equation $L R^\dagger = \mathbb{1}_D$; thus, L is a generalised inverse of R^\dagger . Since R is a $D \times n$ matrix having $|E_k\rangle\rangle$ as columns, it is a rank- D matrix (recall there are only D independent E_k matrices). We can write its singular value decomposition (SVD), i.e., $R = U(\Sigma|\hat{0})W^\dagger$ with $\Sigma = \text{diag}[\sigma_1, \dots, \sigma_D]$ ($\sigma_s > 0$) and $\hat{0}$ being the $D \times (n-D)$ zero-matrix. Having this, a simple exercise shows $L = U(\Sigma^{-1}|H)W^\dagger$ with H being an arbitrary $D \times (n-D)$ matrix. Accordingly, we can split solution into

two parts $L = L^{(p)} + L^{(h)}$, with $L^{(p)} = U(\Sigma^{-1}|\hat{0})W^\dagger$ (particular) and $L^{(h)} = U(\hat{0}|H)W^\dagger$ (homogeneous). This results in a family of equivalent estimators

$$\hat{\eta}_k = \sum_{s=1}^D L_{sk} \hat{B}_s = \sum_{s=1}^D \left(L_{sk}^{(p)} + L_{sk}^{(h)} \right) \hat{B}_s = \hat{\eta}_k^{(p)} + \hat{\eta}_k^{(h)}, \quad (8)$$

parameterised by a homogeneous solution $\hat{\eta}_k^{(h)}$. As we shall see, this multiplicity of possible inversion schemes represents an additional resource for error optimisation in post-processing. We turn to observable properties which may be expressed in terms of estimator coefficients $a_k = \text{Tr}[A \hat{\eta}_k] = a_k^{(p)} + a_k^{(h)}$, with $a_k^{(p/h)} = \text{Tr}[A \hat{\eta}_k^{(p/h)}]$. The homogeneous coefficients, from the definition of $\hat{\eta}_k^{(h)}$ in Eq. (8), do not influence expectation values or any other linear combination of classical shadows

$$\langle a \rangle = \sum_{k=1}^n p_k a_k = \sum_{k=1}^n p_k \left(a_k^{(p)} + a_k^{(h)} \right) = \sum_{k=1}^n p_k a_k^{(p)}. \quad (9)$$

By substituting $p_k = \text{Tr}[\rho E_k]$ and $\langle a \rangle = \text{Tr}[A \rho]$ into the previous equation we find

$$\sum_k a_k^{(p)} E_k = A, \quad (10)$$

$$\sum_k a_k^{(h)} E_k = 0. \quad (11)$$

The set of solutions to the latter (homogeneous) equation defines an auxiliary optimisation space of dimension $n - D$ independent of the target observable (fixed by the choice of POVM). This is a free resource that may now be used in post-processing.

Now, to effectively compare the different choices for estimators, we refer to the efficiency of the estimation process, that is the expected sample size of copies required to estimate a property of the state up to a fixed accuracy. It is customary in classical shadow tomography to refer to variance as figure of merit [1]. In particular, we consider the state-independent upper bound on variance, called *shadow norm* $\|A\|_{\text{sh}}^2$, defined as:

$$\begin{aligned} \text{Var}[a] &= \mathbb{E}[a^2] - (\mathbb{E}[a])^2 \leq \mathbb{E}[a^2] = \sum_{k=1}^n p_k |a_k|^2 \\ &\leq \max_{\sigma: \text{state}} \text{Tr} \left[\sigma \sum_{k=1}^n |a_k^{(p)} + a_k^{(h)}|^2 E_k \right] = \|A\|_{\text{sh}}^2. \end{aligned} \quad (12)$$

Considering the upper bound to study sample complexity is reasonable since, for bounded observables, the quantity $(\mathbb{E}[a])^2$ is also bounded, therefore the relevant contribution is brought by the first term $\mathbb{E}[a^2]$.

This quantity is equivalent to the maximal eigenvalue of the *variance operator* defined as $\hat{O}_A := \sum_{k=1}^n |a_k^{(p)} + a_k^{(h)}|^2 E_k$; we will use both definitions interchangeably. This is akin to

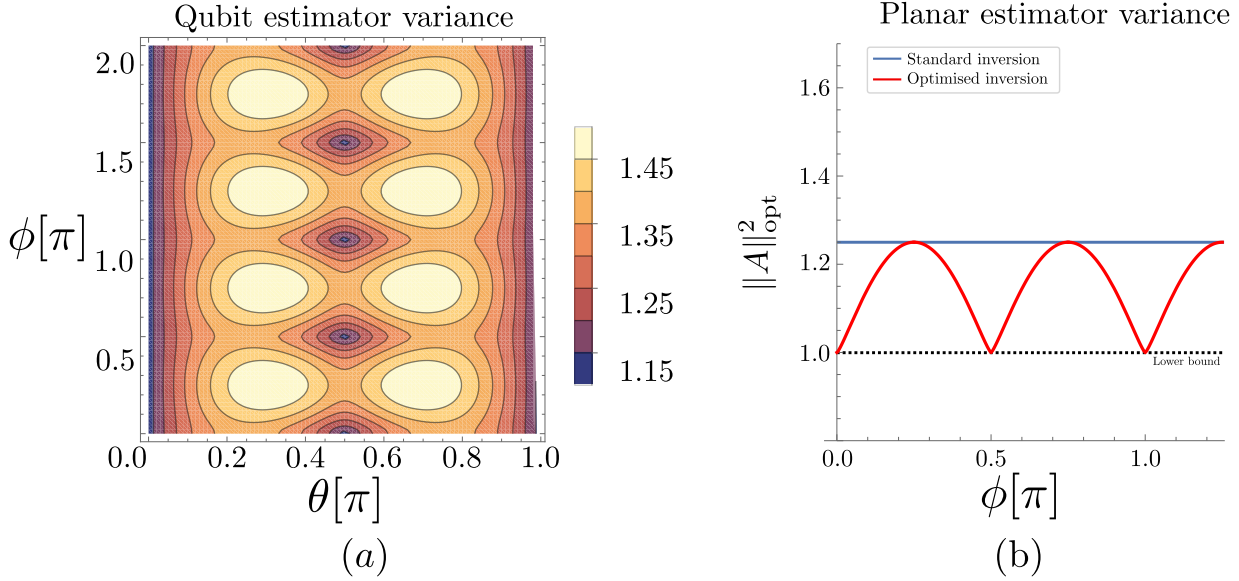


FIG. 2. (a) **Optimal free parameter for projectors on the Bloch sphere.** The contour plot shows the minimal shadow norm Eq. (13) of the single-qubit projector characterised by the Bloch sphere angles θ, ϕ (in units of π). Optimisation results in bounds lower or equal than $3/2$, obtained via the Clifford inversion map Eq. (15) found in [1]. (b) **Optimal free parameter for plane projectors.** The optimal value of the shadow norm of the single-qubit projector in the equatorial plane in terms of a single angle parameter ϕ (in units of π). This enhanced norm takes values in the range $1 \leq \|\psi\rangle\langle\psi|(\phi)\|_{\text{sh}}^2 \leq 5/4$ (see main text). In the case of $\phi = k\frac{\pi}{2}, k \in \mathbb{Z}$, which corresponds to the projectors on the Pauli X and Y basis, the bound achieves optimal value $\|\psi\rangle\langle\psi|(\phi)\|_{\text{sh}}^2 \equiv 1$.

the original upper bound on shadow norm and thence sampling complexity found in [1], where the expected number of samples scales with $M = O(\varepsilon^{-2} \log \delta^{-1} \|A\|_{\text{sh}}^2)$. Nevertheless, this can be further optimised over the free parameters in the homogeneous part of the estimator. By optimising over these coefficients, it is possible to identify the configuration which guarantees the minimal sample size for the estimation of the particular observable A :

$$\|A\|_{\text{opt}}^2 = \min_{a_k^{(h)}: H} \max_{\sigma: \text{state}} \text{Tr} \left[\sigma \sum_{k=1}^n |a_k^{(p)} + a_k^{(h)}|^2 E_k \right], \quad (13)$$

The existence of a minimum is guaranteed through the positive semidefiniteness of the variance operator. We will provide examples to illustrate that different choices of free parameters may result in a sampling complexity with exponential separation compared to that of the naive estimator construction, which shows, in turn, that optimisation in Eq. (13) yields exceptional gains for relatively minuscule cost.

PRODUCT OBSERVABLES AND SHADOW OPTIMISATION

Let us now discuss the estimation of product observables $A^{(N)} = A_1 \otimes A_2 \dots \otimes A_N$ via local POVMs, i.e., of the type $E_{k_1} \otimes \dots \otimes E_{k_n}$. This case is particularly interesting for near-term applications, such as the VQE algorithm [42, 43]. In such a scenario, it is easy to show that the shadow norm in Eq. (12) has a product form (see also [27]) and consequently

Eq. (13) becomes

$$\|A^{(N)}\|_{\text{opt}}^2 = \prod_{j=1}^N \|A_j\|_{\text{opt}}^2 \quad (14)$$

Since we are considering local measurements on independent subsystems, each term $\|A_j\|_{\text{opt}}^2$ can be optimised locally, implying the optimisation in Eq. (14) is efficient overall. We see that even minimal deviation from the minimum in local shadow norms $\|A_j\|_{\text{opt}}^2$ may accumulate exponentially fast with N . This is illustrated in Figure 1(b) for the case of the canonical inversion map of Eq. (15). We now present examples of such exponential improvement for qubits for particular sets of local observables, specifically projectors, whereby by adjusting the available free parameters, we are able to reduce the expected bound on sample size based on assumptions for the observable itself.

FIDELITY ESTIMATION OF PRODUCT STATES

We first consider the case of estimation of fidelity with product states. The target observables are thus tensor products of a projector on a single qubit $\bigotimes_{j=1}^N |\psi_j\rangle\langle\psi_j|$, parameterised on the Bloch sphere by two angles (θ_j, ϕ_j) . The measurement scheme is described by the POVM of normalised projectors on the Pauli basis $E_\zeta^\pm = \frac{1}{6}(\mathbb{1} \pm \sigma_\zeta)$, where $\zeta = x, y, z$. Using the estimators

$$\hat{\eta}_\zeta^\pm = 3 \left(3E_\zeta^\pm - \text{Tr} \left[E_\zeta^\pm \right] \mathbb{1}_2 \right). \quad (15)$$

found in [1], the shadow norm in Eq. (12) simply evaluates for the generic single-qubit observable $A = a \cdot \mathbb{1} + x \cdot \sigma_x + y \cdot \sigma_y + z \cdot \sigma_z$ to

$$\|A\|_{\text{sh}}^2 = a^2 + 3(x^2 + y^2 + z^2) + 2|a|\sqrt{x^2 + y^2 + z^2}. \quad (16)$$

Considering the particular case of projectors on the Bloch sphere, with the parameterisation

$$\begin{aligned} a &\rightarrow \frac{1}{2}, & x &\rightarrow \frac{1}{2} \sin \theta \cos \phi, \\ y &\rightarrow \frac{1}{2} \sin \theta \sin \phi, & z &\rightarrow \frac{1}{2} \cos \theta, \end{aligned} \quad (17)$$

and Eq. (16) trivially reduces to $\|\psi\rangle\langle\psi|\|_{\text{sh}}^2 \equiv \frac{3}{2}$. Now we show how to improve this reference bound by our techniques. The POVMs E_ζ^\pm span the entire HS space and we may determine easily a homogeneous combination of the effects as in Eq. (11) given $\sum_\zeta h_\zeta^+ E_\zeta^+ + h_\zeta^- E_\zeta^- = 0$. Exploiting the symmetry of the system, they reduce to three parameters since $h_\zeta^+ = h_\zeta^-$:

$$\{h_\zeta\}_{\zeta=x,y,z} = \{p_1, p_2, -p_1 - p_2\} \quad (18)$$

As expected, we find $n - D = 2$ parameters p_1, p_2 .

Optimising over these parameters, we present the minimal upper bound as a function of angles (θ, ϕ) in Fig. 2(a). The optimised results are contained within the interval $1.15 \leq \|\psi_j\rangle\langle\psi_j|\|_{\text{sh}}^2 \leq 1.5$. Since the overall shadow norm Eq. (14) is of the product form, there are entire regions in the (θ, ϕ) -space for which deviations from the standard $3/2$ leads to the exponential improvement in N .

ESTIMATION WITH CONSTRAINED POVMs

In the previous section we have studied examples of overcomplete POVMs in the entire HS space, i.e. with $D = d^2$. Here we will pursue a relevant example of a POVM spanning only a subspace \mathcal{V}_D of lower dimension $D < d^2$, in which E_k forms an over-complete basis (within \mathcal{V}_D). Note that the standard inversion procedure [1, 27] is defined on the full HS space and does not directly apply in this instance.

Consider for instance the POVM constituted by the projectors of the X and Y Paulis $E_\zeta^\pm = \frac{1}{4}(\mathbb{1} \pm \sigma_\zeta)$, where $\zeta = x, y$, which spans the "equator" on the Bloch sphere. With a straightforward application of our procedure Eq. (8), we obtain the following particular solution

$$\hat{\eta}_\zeta^\pm = 4E_\zeta^\pm - \text{Tr}[E_\zeta^\pm] \mathbb{1}_2. \quad (19)$$

The homogeneous term is added by solving $\sum_\zeta h_\zeta^+ E_\zeta^+ + h_\zeta^- E_\zeta^- = 0$, where $\{h_\zeta\}_{\zeta=x,y} = \{p, -p\}$ and p is a free parameter. For the generic planar observable (within span of $\{E_\zeta^\pm\}$)

$$A = \begin{pmatrix} a & x + iy \\ x - iy & a \end{pmatrix}, \quad (20)$$

we find the shadow norm

$$\begin{aligned} \|A\|_{\text{sh}}^2(p) &= (a - x)^2 + 2(x^2 + y^2) + B(p) + \sqrt{C(p)}, \\ (21) \end{aligned}$$

$$\begin{aligned} B(p) &= \frac{1}{8}(2(p_r^2 + p_i^2)a^2 + (p_r(8 + p_r) + p_i^2)x^2 \\ &\quad + (p_r(p_r - 8) + p_i^2)y^2), \\ C(p) &= x^2(a(8 + p_r(6 + p_r) + p_i^2) - 2(4 + p_r)x)^2 \\ &\quad + (a(8 + (p_r - 6)p_r + p_i^2) + 2(p_r - 4)x)^2y^2, \end{aligned}$$

where $p_r = \text{Re}\{p\}$ and $p_i = \text{Im}\{p\}$.

We can now proceed to two examples of estimation of product observables via local measurements achieving the same scaling of resources as global strategies [1].

Optimal estimation of planar Paulis

When considering as target observable the planar Pauli,

$$a \rightarrow 0, \quad x \rightarrow \cos \varphi, \quad y \rightarrow \sin \varphi, \quad (22)$$

the optimised shadow norm from Eq. (21) results in $\|A\|_{\text{opt}}^2 = 2$. An immediate result is that the expected number of resources for product of planar Paulis scales as 2^N , which matches the scaling obtained from global Clifford measurements [1], $\|A\|_{\text{sh}}^2 = \text{Tr}[A^2] = 2^N$. Surprisingly, we are able to match the optimal scaling [44] while still relying only on local single-qubit measurements.

Complete versus overcomplete POVMs

In the context of the previous example, it is interesting to compare the performance of complete versus overcomplete POVM. For this purpose, consider the example of a triangle POVM on the plane, defined as the normalised projectors $E_k = \frac{2}{3}|\psi_k\rangle\langle\psi_k|$ of states

$$|\psi_k\rangle = \frac{|0\rangle + e^{i\frac{k}{3}2\pi}|1\rangle}{\sqrt{2}} \quad k = 0, 1, 2 \quad (23)$$

Simple inversion of this complete basis brings us to estimators

$$\hat{\eta}_k = 3E_k - \frac{3}{4}\text{Tr}[E_k] \mathbb{1}_2. \quad (24)$$

Since the POVM is complete, there is no free parameter dependence. From here, we can compute the shadow norm as defined in Eq. (12). For a planar Pauli as target observable, as in Eq. (22), the shadow norm is $\|A\|_{\text{sh}}^2 = 3, \forall \varphi$, which leads to an expected overhead of 3^N on the scaling of resources. From the previous example, the same observables can be optimally estimated with an overhead of 2^N . We have therefore found an example in which an overcomplete POVM performs better than a complete measurement scheme in the same subspace.

Locally efficient fidelity estimation implies globally efficient

We now present a configuration in which the optimisation of the inversion map not only improves the sample complexity, but is actually able to achieve efficient estimation, i.e. $\|A\|_{\text{opt}}^2 = 1$.

To show this, we choose as target observables tensor products of projectors that act on a qubit, $A = \bigotimes_{j=1}^N |\psi(\phi_j)\rangle\langle\psi(\phi_j)|$ where each single-qubit state is parameterised as: $|\psi(\phi_j)\rangle = (|0\rangle + e^{i\phi_j}|1\rangle)/\sqrt{2}$.

Using the change of coordinates

$$a \rightarrow \frac{1}{2}, \quad x \rightarrow \frac{1}{2} \cos \phi, \quad y \rightarrow \frac{1}{2} \sin \phi, \quad (25)$$

we express the generic shadow norm from Eq. (21) in terms of the parameter ϕ :

$$\begin{aligned} \|\langle\psi|\psi\rangle(\phi)\|_{\text{sh}}^2 &= \frac{1}{2}(1 + p_i^2 + B(\phi, p_r) + \sqrt{2}\sqrt{C(\phi, p_r)}) \\ B(\phi, p_r) &= (4p_r - 2)\cos\phi + \cos 2\phi + 2 \\ &\quad + 2p_r(p_r - 1) \\ C(\phi, p_r) &= (4p_r - 1)\cos\phi + 2p_r \cos 2\phi \\ &\quad + \cos 3\phi + 2 + 2p_r(p_r - 1), \end{aligned} \quad (26)$$

where $p_r = \text{Re}\{p\}$, $p_i = \text{Im}\{p\}$. In Fig. 2(b) we present the optimal value of the shadow norm for $\phi \in [0, \pi]$. We note that for each value of ϕ the optimised norm is $\|\langle\psi|\psi\rangle(\phi)\|_{\text{opt}}^2 \leq 5/4$. For angles $\phi = 0, \pi/2, \pi, 3\pi/2$, the optimal shadow norm is exactly $\|E_\zeta^\pm\|_{\text{opt}}^2 = 1$, corresponding to the eigenprojectors of X and Y .

This is particularly relevant considering that X and Y are non-commuting observables, as it opens the possibility of the simultaneous estimation of up to 4^N projections simultaneously for complementary observables. Previously this result has been found in [1] only via global measurement strategies relying on N -qubit Clifford unitaries. We have shown instead that this is achieved using exclusively local measurements.

DISCUSSION

In the course of this letter we have observed how post-processing, an often overlooked aspect in estimation, represents a relevant resource to be examined in the accounting of a more efficient tomography. By introducing a generalised framework to obtain families of equivalent parameter-dependent estimators, we have found a clear relation between over-complete POVMs and their ability to reduce the variance in estimation of arbitrary observables. When considering local measurements on large composite quantum systems, even a small gain on each estimator represents an overall improvement in sample complexity, yielding an exponential separation between the naive sample variance and the optimised

one as seen in Figure 1(b). In the case of example two, this optimised gain can achieve a variance that performs as well as global classical shadows for given observables, with modest additional post processing that remains efficient. We anticipate that by considering overcomplete POVMs containing joint measurements on multiple qubits, further advantage may be found at increased (but still tractable) optimisation difficulty, either in sample complexity or the set of observables. Finally, interleaving optimised multiqubit measurements may yield sample improvements that approach regular classical shadows within some limit. Such questions are natural candidates for further investigation and the identification of such a hierarchy of optimisation will be the topic of future work.

Note - In preparation of this manuscript, we became aware of two other works [45, 46] considering a similar problem. The authors consider a similar optimisation of the post-processing stage in estimation tasks, albeit referring to different frameworks.

ACKNOWLEDGEMENTS

We thank Richard Küng for his insight and excellent discussions on the subject matter. This research was funded in whole, or in part, by the Austrian Science Fund (FWF) [10.55776/F71] (BeyondC). For the purpose of open access, the author(s) has applied a CC BY public copyright licence to any Author Accepted Manuscript version arising from this submission.

* andrea.caprotti@univie.ac.at

† joshua.morris@univie.ac.at

‡ borivoje.dakic@univie.ac.at

- [1] H.-Y. Huang, R. Kueng, and J. Preskill, *Nature Physics* **16**, 1050–1057 (2020).
- [2] S. Aaronson, (2017), 10.48550/ARXIV.1711.01053.
- [3] H.-Y. Hu, S. Choi, and Y.-Z. You, *Phys. Rev. Res.* **5**, 023027 (2023).
- [4] A. Elben, R. Kueng, H.-Y. R. Huang, R. van Bijnen, C. Kokail, M. Dalmonte, P. Calabrese, B. Kraus, J. Preskill, P. Zoller, and B. Vermersch, *Phys. Rev. Lett.* **125**, 200501 (2020).
- [5] H.-Y. Huang, R. Kueng, and J. Preskill, *Phys. Rev. Lett.* **127**, 030503 (2021).
- [6] A. Neven, J. Carrasco, V. Vitale, C. Kokail, A. Elben, M. Dalmonte, P. Calabrese, P. Zoller, B. Vermersch, R. Kueng, and B. Kraus, *npj Quantum Information* **7**, 152 (2021).
- [7] O. Crawford, B. v. Straaten, D. Wang, T. Parks, E. Campbell, and S. Brieler, *Quantum* **5**, 385 (2021).
- [8] S. Chen, W. Yu, P. Zeng, and S. T. Flammia, *PRX Quantum* **2**, 030348 (2021).
- [9] C. Hadfield, S. Bravyi, R. Raymond, and A. Mezzacapo, *Communications in Mathematical Physics* **391**, 951 (2022).
- [10] A. Zhao, N. C. Rubin, and A. Miyake, *Phys. Rev. Lett.* **127**, 110504 (2021).
- [11] A. Seif, Z.-P. Cian, S. Zhou, S. Chen, and L. Jiang, *PRX Quantum* **4**, 010303 (2023).

[12] K. Wan, W. J. Huggins, J. Lee, and R. Babbush, *Communications in Mathematical Physics* **404**, 629 (2023).

[13] R. Levy, D. Luo, and B. K. Clark, *Phys. Rev. Res.* **6**, 013029 (2024).

[14] K. Bu, D. E. Koh, R. J. Garcia, and A. Jaffe, *npj Quantum Information* **10**, 6 (2024).

[15] L. Coopmans, Y. Kikuchi, and M. Benedetti, *PRX Quantum* **4**, 010305 (2023).

[16] C. Bertoni, J. Haferkamp, M. Hinsche, M. Ioannou, J. Eisert, and H. Pashayan, (2023), [arXiv:2209.12924 \[quant-ph\]](https://arxiv.org/abs/2209.12924).

[17] D. E. Koh and S. Grewal, *Quantum* **6**, 776 (2022).

[18] M. McGinley and M. Fava, *Phys. Rev. Lett.* **131**, 160601 (2023).

[19] J. Kunjummen, M. C. Tran, D. Carney, and J. M. Taylor, *Phys. Rev. A* **107**, 042403 (2023).

[20] J. T. Iosue, K. Sharma, M. J. Gullans, and V. V. Albert, *Phys. Rev. X* **14**, 011013 (2024).

[21] K. Nakaji, S. Endo, Y. Matsuzaki, and H. Hakoshima, *Quantum* **7**, 995 (2023).

[22] N. Feldman, A. Kshetrimayum, J. Eisert, and M. Goldstein, *PRX Quantum* **3**, 030312 (2022).

[23] N. Wyderka, A. Ketterer, S. Imai, J. L. Bönsel, D. E. Jones, B. T. Kirby, X.-D. Yu, and O. Gühne, *Phys. Rev. Lett.* **131**, 090201 (2023).

[24] S. H. Sack, R. A. Medina, A. A. Michailidis, R. Kueng, and M. Serbyn, *PRX Quantum* **3**, 020365 (2022).

[25] A. Anshu, S. Arunachalam, T. Kuwahara, and M. Soleimanifar, *Nature Physics* **17**, 931 (2021).

[26] H.-Y. Huang, S. Chen, and J. Preskill, *PRX Quantum* **4**, 040337 (2023).

[27] H. C. Nguyen, J. L. Bönsel, J. Steinberg, and O. Gühne, *Phys. Rev. Lett.* **129**, 220502 (2022).

[28] T. Zhang, J. Sun, X.-X. Fang, X.-M. Zhang, X. Yuan, and H. Lu, *Phys. Rev. Lett.* **127**, 200501 (2021).

[29] G. Struchalin, Y. A. Zagorovskii, E. Kovlakov, S. Straupe, and S. Kulik, *PRX Quantum* **2**, 010307 (2021).

[30] D. Stilck França, L. Markovich, V. Dobrovitski, A. Werner, and J. Borregaard, *Nat Commun.* **15** (2024), doi: 10.1038/s41467-023-44012-5.

[31] M. Ippoliti, Y. Li, T. Rakovszky, and V. Khemani, *Phys. Rev. Lett.* **130**, 230403 (2023).

[32] J. Morris, V. Saggio, A. Gočanin, and B. Dakić, *Advanced Quantum Technologies* **5**, 2100118 (2022), <https://onlinelibrary.wiley.com/doi/pdf/10.1002/qute.202100118>.

[33] A. Glos, A. Nykänen, E.-M. Borrelli, S. Maniscalco, M. A. C. Rossi, Z. Zimborás, and G. García-Pérez, (2022), [arXiv:2208.07817 \[quant-ph\]](https://arxiv.org/abs/2208.07817).

[34] R. Stricker, M. Meth, L. Postler, C. Edmunds, C. Ferrie, R. Blatt, P. Schindler, T. Monz, R. Kueng, and M. Ringbauer, *PRX Quantum* **3**, 040310 (2022).

[35] B. Vermersch, M. Ljubotina, J. I. Cirac, P. Zoller, M. Serbyn, and L. Piroli, (2023), [arXiv:2311.08108 \[quant-ph\]](https://arxiv.org/abs/2311.08108).

[36] H.-Y. Huang, M. Broughton, J. Cotler, S. Chen, J. Li, M. Mohseni, H. Neven, R. Babbush, R. Kueng, J. Preskill, and J. R. McClean, *Science* **376**, 1182 (2022), <https://www.science.org/doi/pdf/10.1126/science.abn7293>.

[37] G. García-Pérez, M. A. Rossi, B. Sokolov, F. Tacchino, P. K. Barkoutsos, G. Mazzola, I. Tavernelli, and S. Maniscalco, *PRX Quantum* **2**, 040342 (2021).

[38] Z. Webb, (2016), [arXiv:1510.02769 \[quant-ph\]](https://arxiv.org/abs/1510.02769).

[39] H. Zhu, *Phys. Rev. A* **96**, 062336 (2017).

[40] L. Innocenti, S. Lorenzo, I. Palmisano, F. Albarelli, A. Ferraro, M. Paternostro, and G. M. Palma, *PRX Quantum* **4**, 040328 (2023).

[41] J. Morris and B. Dakić, (2020), [arXiv:1909.05880 \[quant-ph\]](https://arxiv.org/abs/1909.05880).

[42] A. Peruzzo, J. McClean, P. Shadbolt, M.-H. Yung, X.-Q. Zhou, P. J. Love, A. Aspuru-Guzik, and J. L. O'Brien, *Nature Communications* **5** (2014), 10.1038/ncomms5213.

[43] J. Tilly, H. Chen, S. Cao, D. Picozzi, K. Setia, Y. Li, E. Grant, L. Wossnig, I. Rungger, G. H. Booth, and J. Tennyson, *Physics Reports* **986**, 1–128 (2022).

[44] H.-Y. Huang, R. Kueng, and J. Preskill, *Phys. Rev. Lett.* **126**, 190505 (2021).

[45] J. Malmi, K. Korhonen, D. Cavalcanti, and G. García-Pérez, (2024), [arXiv:2401.18049 \[quant-ph\]](https://arxiv.org/abs/2401.18049).

[46] L. E. Fischer, T. Dao, I. Tavernelli, and F. Tacchino, (2024), [arXiv:2401.18071 \[quant-ph\]](https://arxiv.org/abs/2401.18071).